



Universiteit
Leiden
The Netherlands

Effects of ozone on stratum corneum lipid integrity and assembly

Petracca, B.; Nădăban, A.; Eeman, M.; Gooris, G.S.; Bouwstra, J.A.

Citation

Petracca, B., Nădăban, A., Eeman, M., Gooris, G. S., & Bouwstra, J. A. (2021). Effects of ozone on stratum corneum lipid integrity and assembly. *Chemistry And Physics Of Lipids*, 240. doi:10.1016/j.chemphyslip.2021.105121

Version: Publisher's Version

License: [Licensed under Article 25fa Copyright Act/Law \(Amendment Taverne\)](#)

Downloaded from: <https://hdl.handle.net/1887/3214416>

Note: To cite this publication please use the final published version (if applicable).



Contents lists available at ScienceDirect

Chemistry and Physics of Lipids

journal homepage: www.elsevier.com/locate/chemphyslip

Effects of ozone on stratum corneum lipid integrity and assembly

Benedetta Petracca^{a,b}, Andreea Nădăban^c, Marc Eeman^{a,*}, Gert S. Gooris^c, Joke A. Bouwstra^c

^a Dow Silicones Belgium SRL, Rue Jules Bordet, Parc Industriel Zone C, B-7180 Senefte, Belgium

^b Adolphe Merkle Institute, University of Fribourg, Chemin des Verdiers 4, CH-1700 Fribourg, Switzerland

^c Division of Biotherapeutics, Leiden Academic Centre for Drug Research, Leiden University, 2333 CC Leiden, the Netherlands

ARTICLE INFO

Keywords:

Stratum corneum
Skin
Ozone
Pollution
Oxidation
Lipids
Ceramides

ABSTRACT

The stratum corneum (SC) acts as the main barrier of the skin against exogenous substances (e.g. air pollutants) and against the loss of endogenous substances such as water. The SC consists of keratin-rich dead cells surrounded by crystalline lamellar lipid regions. The main lipid classes are ceramides (CERs), free fatty acids (FFAs), and cholesterol (CHOL).

Tropospheric ozone (O₃) is a potent oxidant compound that reacts instantly with biological molecules such as lipids and proteins. Although it has been reported that O₃ induces biological responses at the cellular level, to the best of our knowledge, there is no information related to the damages O₃ can cause at the level of the SC extracellular lipid matrix.

The aim of our work was to investigate which SC lipid subclasses are prone to oxidation when exposed to O₃ and how the changes in chemical structures affect the lipid organization in a stratum corneum substitute (SCS) membrane. Ultimately, the barrier properties of the SCS were examined.

Our studies revealed that O₃ induces chemical modifications of the unsaturated bonds in CERs and CHOL. The appearance of carbonyl groups at the headgroup level and the removal of the linoleate moiety of omega-O-acylceramides (CER EOS) impact the lamellar organization of the lipid assembly and to a lesser extent the lateral packing of the lipids. Unexpectedly, these changes improved the barrier function of the SCS.

1. Introduction

Being at the interface with the environment, the skin protects the human body against external aggressors such as solar radiation, tropospheric ozone (O₃), polycyclic aromatic hydrocarbons, volatile organic compounds, particulate matter, and cigarette smoke (Krutmann et al., 2017; Drakaki et al., 2014).

The outermost layer of the skin, the stratum corneum (SC), plays a crucial role in the skin barrier function. This 15–20 μm thick layer is formed by dead cells (corneocytes) that are the terminal differentiation phenotype of keratinocytes, the main cell component of the underlying viable epidermis. The SC structure is often described as a ‘brick and mortar’ model in which corneocytes (bricks) are embedded in a highly organized lipid matrix (mortar) (Wertz et al., 1985; Pouillot et al., 2008). The binding of the extracellular lipid matrix to the corneocytes is ensured by the cornified envelope, a dense network of crosslinked proteins surrounded by a lipid monolayer, that makes the corneocytes less permeable to several exogenous substances. The lipid monolayer acts as an interface between the corneocytes and the extracellular lipids and is

important for the skin barrier function (Meguro et al., 2000; Swartzendruber et al., 1987; Krieg et al., 2013). Thus, exogenous molecules preferably penetrate through the extracellular lipid matrix whose composition and organization have been studied extensively (Pouillot et al., 2008; Elias, 2005).

The extracellular lipid matrix of the human SC is primarily composed of ceramides (CERs), cholesterol (CHOL) and free fatty acids (FFAs) in an approximately equimolar molar ratio, but shows high inter-subject variability (Van Smeden et al., 2011). Nowadays CERs can be classified into 18 subclasses according to the characteristics of their sphingoid base and acyl chain. Moreover each of these subclasses shows a broad carbon chain length distribution (Van Smeden et al., 2011; Van Smeden and Bouwstra, 2016; T'Kindt et al., 2012; Rabionet et al., 2014; Masukawa et al., 2009). The chain length distribution in FFAs in human SC is also significant (Norlén et al., 1998).

Several X-ray diffraction studies showed that SC lipids form two co-existing lamellar phases with repeat distances of around 13 and 6 nm, which are referred to as long and short periodicity phases, named LPP and SPP respectively (Ohta et al., 2003; Bouwstra et al., 1991). The LPP

* Corresponding author.

E-mail address: marc.eeman@dow.com (M. Eeman).

<https://doi.org/10.1016/j.chemphyslip.2021.105121>

Received 23 April 2021; Received in revised form 4 July 2021; Accepted 30 July 2021

Available online 3 August 2021

0009-3084/© 2021 The Dow Chemical Company. Published by Elsevier B.V. All rights reserved. This is an open access article under the CC BY-NC-ND license

(<http://creativecommons.org/licenses/by-nc-nd/4.0/>).

plays a crucial role in the skin barrier function and permeability (De Jager et al., 2006a; Opálka et al., 2020). The most prevalent lateral packing formed by lipids in human SC is the very dense orthorhombic (ORTH) structure, while a smaller proportion of lipids forms a less densely packed hexagonal (HEX) (Boncheva, 2014; Pilgram et al., 1999). Studies using SC lipid assemblies showed a similar lateral organization, but in these model systems the presence of a small portion of disordered liquid (LIQ) phase has also been reported that is very hard to detect in intact SC (Bouwstra et al., 2001). Fig. 1A shows a schematic overview of the epidermal structure, and of the SC lipid organization and composition.

Among the pollutants to which the skin is exposed in daily life, O_3 is one of the most powerful known oxidants as it quickly reacts with

biological targets such as lipids and proteins (Bocci, 2010). Hence, tropospheric O_3 is in principle hazardous to all living organisms on earth (Cross et al., 2002). Being a highly reactive molecule, O_3 cannot penetrate the inner layers of the human skin (Valacchi et al., 2012; Pryor, 1992). However, the reaction products formed by the ozonolysis of lipids and proteins can act as signalling molecules, penetrate into the lower layers of the skin and cause further damage (Valacchi, 2010; Petracca et al., 2021). In particular, the addition of an O_3 molecule to an olefinic C—C double bond forms an intermediate called 1,2,3-trioxolane, which rearranges to an ozonide by the Criegee mechanism (Pryor et al., 1995a; Bailey, 1958; Criegee, 1975). In presence of water, the ozonide decomposes to yield aldehydes and hydroperoxides (Bailey, 1958; Pryor et al., 1995b, c; Pryor and Church, 1991). Several CER

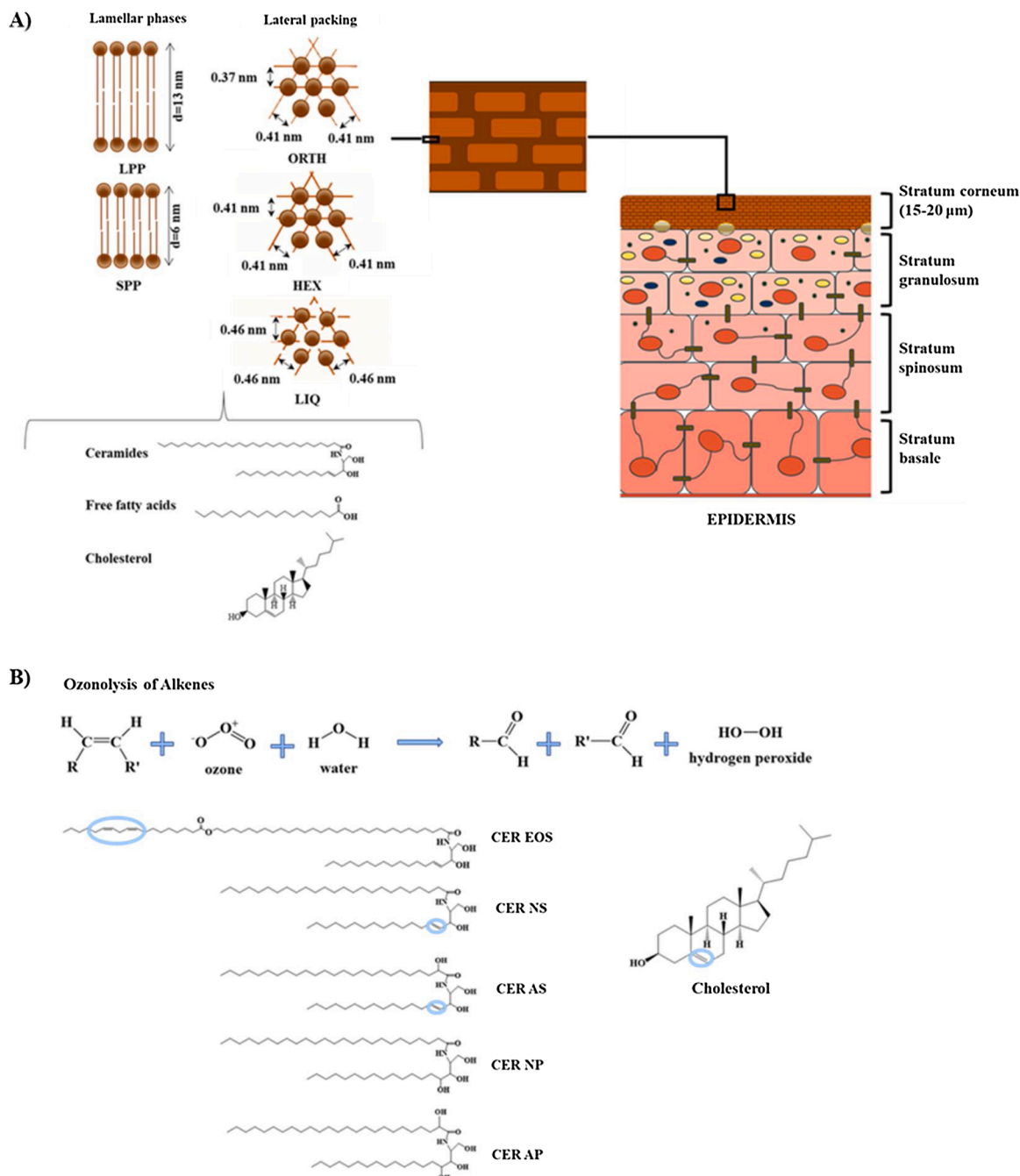


Fig. 1. A) Schematic overview of the skin structure highlighting the main components of the extracellular lipid matrix and their spatial organization in terms of lamellar arrangement and lateral packing. B) Chemical structure of CERs and CHOL used in our SCS membrane (blue circles indicating the portion subjected to ozonolysis) and the net reaction of O_3 with unsaturated lipid molecules in presence of water.

subclasses in the SC are characterized by olefinic C—C double bonds and are believed to be highly sensitive to oxidation. In particular, we hypothesize that the ester-linked ω -hydroxyl acyl chain (EO) with a sphingoid base is most susceptible to oxidation as there is a linoleate moiety in a pseudo-fluid phase within the LPP structure (Groen et al., 2010). A well-known member of this ceramide class is an EO chain linked to sphingosine (S), referred to as CER EOS. Fig. 1B shows the proposed mechanism by which O₃ reacts with the olefinic C—C double bonds of the SC lipid constituents.

Several studies explored the noxious effects of O₃ on skin biological responses (Thiele et al., 1997; Fuks et al., 2019; Rasmussen et al., 2010; Valacchi et al., 2004). However, to the best of our knowledge, there is so far no literature reporting the impact of O₃ on both the chemical structure and biophysical properties of SC lipids. The aim of this work is to understand how ozonation of the lipids in the SC extracellular matrix can impact the organization and consequently the barrier function of the skin. As a first step we used lipid membrane models, referred to as stratum corneum substitute (SCS). This is a multi-layered lipid assembly that mimics several important aspects of both the composition and organization of the SC lipid matrix. SCSs are prepared by spraying on a porous substrate a mixture of CERs, CHOL, and FFAs followed by an equilibration at elevated temperatures to reach phase equilibrium within the SCS (Groen et al., 2008). The lipid models successfully reproduced the lipid organization of the SC, using isolated CERs, CHOL and FFAs (Bouwstra et al., 2001, 1996).

Interestingly, it has been reported that a limited number of synthetic CERs, mimicking human or pig CER composition or even a less variety of CER subclasses, revealed a very similar phase behaviour to that observed in native human and pig skin (De Jager et al., 2004; Groen et al., 2009; De Jager et al., 2005). The use of synthetic lipids can solve problems related to the extraction of native isolated lipids such as inter-individual variability in composition. Furthermore, by using synthetic CER subclasses, the composition of the lipid matrix can be varied on demand (De Jager et al., 2004).

In this work, the lipid mixture used to build SCSs was composed of synthetic CERs, CHOL and FFAs, similarly to previous studies (Opálka et al., 2020; De Jager et al., 2005; Caussin et al., 2008; Van Smeden et al., 2014). The lipid mixture was first exposed to either O₃ or air (negative control) and then sprayed and equilibrated to build a SCS. Changes in lipid composition and organization of the lipid assembly were evaluated. Moreover, the impact of O₃ on the barrier integrity of the membrane model was monitored using ethyl-p-aminobenzoate (E-PABA) as a reference compound. Our results showed that O₃ oxidizes both the unsaturated CERs and CHOL. These chemical changes significantly impacted the lamellar phases and to a lesser extent the lateral packing of the lipids. Unexpectedly, the flux of E-PABA across the O₃ exposed SCS membrane was reduced.

2. Materials and methods

2.1. Materials

The synthetic CER subclasses were kindly donated by Evonik. These are the linoleic acid ester-linked ω -hydroxy acyl chain with 30 carbons (EO, C30) linked to a sphingosine base (S, C18), referred to as CER EOS (C30); a non-hydroxy acyl chain with 24 carbons (N, C24) linked to a S base, referred to as CER NS (C24); a non-hydroxy acyl chain (N, C24 or C16) linked to a phytosphingosine base (P, C18), referred to as CER NP (C24) and CER NP (C16), respectively; an α -hydroxy acyl chain (A, C24) linked to a S base, referred to as CER AS (C24); and an α -hydroxy acyl chain (A, C24) linked to a P base, referred to as CER AP (C24). CER AS and CER AP (D-configuration) isomeric R forms were used. An internal standard (ISTD, provided by Evonik Industries, Essen, Germany) of deuterated CER NS (deuterated C24 acyl chain linked to a protiated C18 sphingoid base) was also used. The CERs had a purity $\geq 90\%$. The FFAs (C16:0, C18:0, C20:0, C22:0, C24:0), ethyl-p-aminobenzoate, referred to

as E-PABA, CHOL and deuterium oxide were supplied by Sigma-Aldrich Chemie GmbH (Schnelldorf, Germany). The deuterated free fatty acids (DFFAs) (C16:0, C18:0, C22:0) were supplied by Larodan (Malmö, Sweden), DFFA (C20:0) and DFFA (C24:0) were obtained from Cambridge Isotope Lab Inc. (Tewksbury, MA, USA) and ARC laboratories (Apeldoorn, The Netherlands), respectively. Sodium acetate (D3, 99 %) and acetic acid (D4, 99.5 %) were purchased from Cambridge Isotope Lab Inc. (Tewksbury, MA, USA). All organic solvents were purchased from Labscan (Dublin, Ireland). All analytical solvents were HPLC grade or higher: n-heptane and chloroform were purchased from Sigma-Aldrich (Sigma-Aldrich, Darmstadt, Germany), while ethanol and isopropyl alcohol were obtained from Biosolve BV (Valkenswaard, The Netherlands). The nucleopore polycarbonate membrane disks (0.05 μm pore size) were purchased from Whatman (Kent, UK). Ultrapure water was obtained through a Milli-Q water purification system (Millipore, Bedford, MA, USA).

2.2. Lipid mixture composition

CERs, FFAs and CHOL in equimolar ratio were dissolved in chloroform : methanol (2 : 1) at a total concentration of 4.45 mg/mL. The following CER composition was selected: CER EOS, CER NS, CER NP (C24), CER AS, CER NP (C16) and CER AP in a 40: 36: 11.3: 2.8: 6.3: 3.5 M ratio. Such ratio mimics the CER subclass composition in pig SC (Bouwstra et al., 1996; De Jager et al., 2005), except for the level of CER EOS that was increased to 40 % to assure that the lipids adopt to only the LPP (Uche et al., 2019a; Gooris et al., 2018). For the FFA mixture, the following saturated fatty acids were selected: C16:0, C18:0, C20:0, C22:0, C24:0 in a 1.8: 4.0: 7.6: 47.8: 38.8 M ratio (Shelley, 1992). An additional model was prepared in which FFAs were replaced by their deuterated counterparts (DFFAs).

2.3. Exposure conditions

Since O₃ is a highly reactive molecule and hardly penetrates the SC (Pryor, 1992; Pryor et al., 1995a), only a thin (i.e., $\sim 5\ \mu\text{m}$) layer of SC lipids was exposed to either O₃ or filtered air (control samples). The sample was prepared by spraying 0.45 mg of the lipid solution over a $10 \times 10\ \text{cm}$ area on a silicon wafer disk (Okmetic, Vantaa, Finland) using a Linomat IV device (Camag, Muttenz, Switzerland) with an extended y-axis arm under a gentle stream of nitrogen. Spraying rate was set at 5 $\mu\text{L}/\text{min}$ and 1 mm distance was maintained between the syringe needle tip of the Linomat device and the silicon wafer surface. If not immediately used, the sprayed silicon wafers were stored under argon. Exposure of the sprayed silicon wafers to either O₃ or filtered air took place in a 40L chamber with controlled ambient conditions (32 °C and 30–40% relative humidity, RH) for 8 h.

O₃ was produced by an electrical corona arc discharge system supplied by air (ECO3 srl, Brandizzo, Italy). O₃ concentration in the chamber was adjusted with a potentiometer and monitored with two O₃ detectors mounted at the inlet and outlet of the chamber, respectively. Lipid samples were exposed to 3.6 ppm of O₃. These concentrations are far from the tropospheric O₃ concentrations found in polluted areas (i.e. 0.35 ppm in severe polluted episodes) (Petracca et al., 2021; Feng et al., 2015). However, higher concentrations were selected to simulate the effects of O₃ chronic exposure and to mimic the worst-case scenario in which the SCS model is composed of fully ozonized lipid mixtures.

Immediately after exposure to either O₃ or filtered air, the lipids constituents were extracted from the silicon wafers by dissolution in chloroform : methanol (2 : 1). To remove any contamination (i.e. dust), the extracted lipid solutions were filtered using a 0.45 μm PVDF filter (Grace, Deerfield IL, USA). Then, the organic solvent was evaporated under nitrogen flow at 40 °C.

Finally, the dried lipids were dissolved in the appropriate solvent and concentration required for liquid chromatography-mass spectrometry (LC-MS), Fourier transform infrared spectroscopy (FTIR), small angle X-

ray diffraction (SAXD) or permeability studies.

2.4. LC-MS samples preparation and analysis

Dried lipids exposed to either O₃ or filtered air were reconstituted in a solution of heptane : chloroform : methanol (95 : 2.5 : 2.5) at a concentration of 0.05 mg/mL. An internal standard (ISTD) of deuterated CER NS (perdeuterated C24 acyl chain linked to a protiated C18 sphingoid base) was added to the samples. For each vial, 3 pmol of lipids were injected in the LC-MS system.

The injected lipids were analysed using an Acquity UPLC H-class (Waters, Milford, MA, USA) connected to a XEVO TQ-S mass spectrometer (Waters, Milford, MA, USA) equipped with an atmospheric pressure chemical ionization (APCI) source. In particular, changes in CER composition and CHOL were studied because of their susceptibility to O₃. The details of the LC-MS analysis method are described elsewhere (Boiten et al., 2016). Briefly, separation of the CERs was performed on a PVA-Sil column (5 µm particles size, 100 × 2.1 mm i.d., YMC, Kyoto, Japan) applying a gradient elution starting at 98 % mobile phase A (100 % heptane) towards 50 % mobile phase B (heptane : isopropyl alcohol : ethanol, 50 : 25 : 25) with a flow rate of 0.8 mL/min. Detection occurred in positive ion mode with a full scan *m/z* measurement between 350–1200 atomic mass units (amu). To monitor the run stability, three quality control (QC) samples of a standard lipid mixture (0.05 mg/mL) were analysed after every 10 samples.

After a manual inspection of each chromatogram, automated peak detection and area integration were performed using the Waters MassLynx and TargetLynx software (v. 4.1). Peak areas under the peak (AUC) were used to analyse the CER species and CHOL. These were corrected for the ISTD.

Furthermore, CER fragments that were produced during the lipid ozonation process were analysed. As O₃ is expected to oxidize olefinic C=C double bonds, the molecular weight (MW) of the sphingosine-based CER fragments was calculated. As APCI was used as an ionization source, only single positively charged ions were measured and could be identified as [M+H]⁺, water loss ions [M+H-H₂O]⁺ or potassium adducts [M + K]⁺.

2.5. FTIR experiments

Dried lipids exposed to either O₃ or filtered air were reconstituted in a mixture of chloroform : methanol (2 : 1) at a concentration of 4.45 mg/mL. SCS samples were prepared by spraying 0.9 mg of the lipid solution over a 10 × 10 mm area on a AgBr window using the Linomat IV device as described previously. Samples were equilibrated for 30 min at 85 °C to ensure the lipid mixtures had fully melted and then gradually cooled down to room temperature (25 °C). Samples were then hydrated with deuterated acetate buffer (pH 5.0) for at least 15 h at 37 °C.

FTIR spectra were acquired using a Varian 670-IR spectrometer (Agilent Technologies, Inc., Santa Clara, CA, USA) equipped with a broad-band mercury cadmium telluride detector, cooled by liquid nitrogen. The samples were continuously purged under dry air, starting from 30 min before data acquisition. The spectra were collected in transmission mode and acquired by the coaddition of 256 scans at 1 cm⁻¹ resolution, over 4 min. To investigate the thermotropic phase behaviour and conformational ordering, the samples were measured between 0 and 90 °C at a heating rate of 0.25 °C/min (1 °C temperature rise per recorded spectrum). The spectra were deconvoluted using a half-width of 4 cm⁻¹ and an enhancement factor of 1.4 using the Varian Resolution Pro software. Samples were measured over a range of 600–4000 cm⁻¹. The CH₂ symmetric stretching modes (2845–2855 cm⁻¹) and the CD₂ symmetric stretching modes (2080–2100 cm⁻¹), termed ν_s CH₂ and ν_s CD₂ respectively, were selected to examine the lipid phase transitions and to determine the lipid mixing properties. The linear regression curve fitting method was used to determine the mid-transition temperature as described elsewhere (Oguri et al., 2014).

The CH₂ rocking vibration mode (719–730 cm⁻¹) and scissoring mode (1462–1473 cm⁻¹), referred to as ρ CH₂ and δ CH₂ respectively, were evaluated to monitor the lateral lipid packing. The CD₂ scissoring modes (~1088 cm⁻¹), referred to as δ CD₂, were analysed to evaluate the mixing properties of the lipid chains. The scissoring peaks at 10 °C and 32 °C were fitted using a sum of Lorentzian functions (Mojumdar et al., 2015). The area of each peak contributing to the total peak area was then calculated. The δ CH₂ mode can be used to monitor the degree of ORTH and HEX lateral packing. The area of the central peak (~1467 cm⁻¹) is a measure for the amount of lipids in a HEX lateral packing, while the areas of the peaks at 1463 and 1473 cm⁻¹ are a measure for the amount of lipids in an ORTH lateral packing. A higher ratio between the sum of the areas at 1463 and 1473 cm⁻¹ and the area of the 1467 cm⁻¹ peak demonstrates a higher fraction of lipids in an ORTH lateral packing. Multiple measurements of the samples were made for each condition (n = 3).

2.6. SAXD study

Dried lipids exposed to either O₃ or filtered air were reconstituted in 200 µL of a hexane : ethanol (2 : 1) solution at a concentration of 4.45 mg/mL. SCS samples were prepared by spraying 0.9 mg of the lipid solution over a 2 × 3 mm area on a nucleopore polycarbonate filter disk with 0.05 µm pore size, using the Linomat IV device as described previously. Samples were equilibrated at 85 °C for 30 min and slowly cooled to room temperature (25 °C). Samples were stored under argon until measurement.

In order to examine the lamellar organization of SCS samples, SAXD measurements at a synchrotron radiation source were performed. We used beamline BL11-NCD-SWEET at ALBA (Cerdanyola del Vallés, Barcelona, Spain). SAXD images were collected using a Pilatus 1 M detector with 981 × 1043 pixels of 172 µm spatial resolution. The X-ray wavelength was set at 0.099987 nm. The sample-to-detector distance was set at 2.148 m. The samples were hydrated for more than 48 h in a hydration chamber at 80 % RH, prior to mounting in a sample holder oriented perpendicular to the primary beam at a temperature of 23 °C. The diffraction patterns of the samples were acquired in one position. The samples were measured for 20 s. The scattering intensity (I) was plotted as a function of the scattering vector (q). The latter is defined as $q = (4\pi \sin \theta) / \lambda$, where 2θ is the angle between the primary beam and the scattered X-rays and λ is the wavelength. From the positions of a series of equidistant peaks (q_n), the periodicity of a lamellar phase was calculated using the equation $d = 2n\pi/q_n$ in which n is the order of the diffraction peak. Multiple samples were measured for each condition (n = 2).

2.7. Permeability studies

Dried lipids exposed to either O₃ or filtered air were reconstituted in 200 µL of a hexane : ethanol (2 : 1) solution at a concentration of 4.45 mg/mL. SCS samples were prepared by spraying 0.9 mg of the lipid solution over a 10 × 10 mm area on a nucleopore polycarbonate filter disk with 0.05 µm pore size using the Linomat IV device as described previously. SCS samples were equilibrated at 85 °C for 30 min and slowly cooled to room temperature (25 °C). The polycarbonate filter only acts as a support for the lipid film. It does not affect the diffusion properties of model permeants. The formation of a lipid assembly on top of the polycarbonate filter and the absence of lipid material inside the pores or at the bottom side of the filter were previously investigated by cryo-scanning electron microscopy (De Jager et al., 2006b).

The permeation studies were performed using in-line diffusion cells (PermeGear, Bethlehem, PA), as described previously (Uche et al., 2019a), with a diffusion area between the donor and acceptor compartments of 0.282 cm². The acceptor medium was made of 0.1 M phosphate buffer saline (PBS) solution prepared by adding NaCl, Na₂HPO₄, KH₂PO₄, and KCl in ultrapure water at a concentration of 8.13, 2.87, 0.20, and 0.19 g/L, respectively. The pH of the buff ;er

solution was adjusted to 7.4 and subsequently filtrated. The donor medium was made of 0.65 mg/mL of E-PABA (saturated solution) in acetate buff ;er. The acetate buffer (pH 5.0) was obtained by adding sodium acetate trihydrate and acetic acid at a concentration of 27.07 g/L and 1.14 vol%, respectively.

SCS samples were mounted between the two compartments of the diffusion cells. The acceptor compartment was then filled with PBS and the SCS samples were let to be hydrated during 1 h. 1400 µL of E-PABA solution was applied on top of each SCS sample, within the donor compartment. An adhesive tape was placed on the donor compartment to maintain occlusive conditions throughout the experiment. The acceptor phase was perfused at a flow rate of approximately 2 mL/h with a flow pump (Ismatec IPC pump; IDEX Health & Science GmbH, Germany) through an in-line degasser (Biotech, Sweden) to remove any air bubbles in the system. The acceptor compartment was stirred with a magnetic stirrer bar (Hengstler, Germany) at 120 rpm. A fraction collector (Isco Retriever IV; Teledyne Isco, Lincoln, NE, USA) was used to collect the acceptor fluid in 10 mL glass vials. The collection time interval was 1 h. The flux was measured over a period of 16 h. During the permeation studies, the temperature of the diffusion cells was kept at a physiological skin temperature of approximately 32 °C and controlled by a thermostated water bath (Lauda Dr. Wobser GmbH; Lauda-Koenigshofen, Germany). After the diffusion studies, the volume per collected fraction was weighted. The flux (amount of E-PABA that penetrates per cm²/h) was calculated using the formula $J = m / (A \times \Delta t)$, in which m is the weight of volume collected, A is the diffusion area (i.e. 0.282 cm²) and Δt is the collection time interval (i.e. 1 h). The permeation of E-PABA across the different SCS samples was performed at least four times ($n \geq 4$) per condition. The steady-state flux was calculated from the plots of E-PABA flux values versus time as average of the flux values measured from the 9th to the 16th hour.

The analysis of E-PABA was carried out using the Acquity Ultra High-Performance Liquid Chromatography (UPLC) systems (Waters Co., Milford, MA, USA) as described elsewhere (Uche et al., 2019a, b). In brief, 10 µL of each sample was injected in the C18 reversed phase column (Alltima, 5 µm i.d., 4.6 × 150 mm). The column temperature was set at 40 °C. The mobile phase used for the UPLC analysis was: 0.1 % trifluoroacetic acid in acetonitrile : ultrapure water at a 40:60 (v/v) ratio. The flow rate of the mobile phase was set to 0.5 mL/min. A UV-detection wavelength of 269 nm was used for E-PABA detection. A standard curve was determined from serial dilutions of a 0.5 mg/mL E-PABA stock solution in a 1:1 solution of methanol and ultrapure water. Data were collected and processed by Waters MassLynx and TargetLynx software (v4.1).

2.8. Data analysis

Statistical analysis was performed using GraphPad Prism 8.0. Unpaired two-tailed *t*-test was performed, with a significance level of $p < 0.05$.

3. Results and discussion

3.1. O₃ modifies SC lipid composition

The impact of O₃ on the SC lipid composition was investigated by exposing thin layers of SC lipids (CERs, FFAs and CHOL) to either 3.6 ppm O₃ or filtered air for 8 h, and by quantifying the changes in lipid species by LC–MS. We focused the analysis on the changes in CERs and CHOL because of their susceptibility to O₃. We decided to study lipid mixtures containing 40 mol% CER EOS of the total CER amount as with such a mixture the lipids form only the LPP that is unique to the SC and important for the skin barrier (Groen et al., 2010; Uche et al., 2019a; Mojumdar et al., 2015; Beddoes et al., 2018; Opálka et al., 2016). Furthermore, as we expected the linoleate moiety of CER EOS to be primarily affected by O₃ we created a lipid system being sensitive to O₃

exposure.

Data are presented as AUC of each lipid corrected for the AUC of the ISTD peak. Fig. 2A shows the amount (AUC) of each CER subclass and CHOL measured after exposure of the SC lipid mixtures to O₃ or filtered air. The results indicate that O₃ affects all unsaturated lipids (i.e. CER EOS, CER AS, CER NS and CHOL). The amount of CER EOS in O₃ exposed samples decreases 12-fold compared to the air exposed samples. O₃ also induces a 2-fold decrease of the amounts of CER AS and CER NS compared to the air exposed samples. The amount of CHOL also decreased 6-fold in the lipid mixture exposed to O₃, probably due to the unsaturated bonds in the structure. Unexpectedly, the amount of the saturated CER NP (C16) decreased 1.2-fold in the O₃ exposed samples, as compared to the lipid samples exposed to air. CER AP and CER NP (C24) amounts did not decrease.

The LC–MS analysis method is also suitable for the identification of some of the lipid fragments that could be formed upon ozonolysis. The MW of these lipid fragments were calculated considering that each olefinic C–C double bond in the molecule would result in the formation of aldehydes upon ozonolysis (Criegee, 1975), and used for the identification during data analysis. The ozonolysis fragments of CER NS (MW 469.5) and CER AS (MW 485.5) were detected in the O₃ exposed samples at a retention time of 6.3 min and 7.6 min, respectively. The only fragment detected for CER EOS was the fragment obtained from the ozonolysis of the C–C double bond of the linoleate chain (MW 904), with a retention time of 4.5 min.

The ionization of the LC–MS method determines the formation of different ions: mainly proton adducts $[M+H]^+$ and water loss fragments of the proton adduct ion $[M+H-H_2O]^+$ and $[M+H-2H_2O]^+$, as described elsewhere (Boiten et al., 2016). The abundance of these ions is reported to be dependent on the CER subclass. Therefore, the main ion detected for CER NS and CER AS fragments is $[M+H-H_2O]^+$ (m/z 452.5 and 468.5, respectively), with a low abundance of the $[M+H]^+$ ion detected at m/z 470.5 (CER NS fragment) and m/z 486.5 (CER AS fragment). CER EOS fragment is characterized by the $[M+H-H_2O]^+$ ion with m/z 886.9 and the $[M+H]^+$ ion with m/z 905. Fig. 2B shows the spectrum of each CER fragment ion mentioned above, at the corresponding retention time of each fragment. No fragments corresponding to CER NP (C16), CER NP (C24) and CER AP were detected in the O₃ exposed samples. Even though the concentration of CER NP (C16) appeared to be lower in the O₃ exposed samples compared to the air exposed samples, the LC–MS analysis did not identify any fragments that would suggest a possible ozonolysis of this saturated CER species. As CER NP (C16) is present at a low concentration in the lipid assembly, the reduced amount observed in the O₃ exposed condition could arise from sample inter-variability. It is worth noting that none of the above mentioned CER fragments were detected in the air exposed samples.

Although the amount of CHOL is strongly decreased in SC lipid samples exposed to O₃, no fragment resulting from the ozonolysis of CHOL could be detected because their MW is below the m/z scanning range of our LC–MS method.

To the best of our knowledge, still little is known about the impact of O₃ on both the chemical structure and assembly properties of SC lipids. However, previous studies showed that SC lipid-based liposomes exposed to a combination of ultraviolet radiation (UV) and transition metal ions undergo lipid peroxidation primarily at the level of unsaturated fatty acids and cholesterol (Trommer et al., 2003; Trommer, 2001). Whereas in those studies no oxidation was detected in cholesterol sulphate samples, they also highlight the importance of the presence of unsaturated lipid molecules in SC membrane models on the oxidation potential of external factors such as air pollutants and UV radiation.

3.2. O₃ influences SCS thermotropic response

An optimal lipid packing and high conformational ordering are crucial for the skin barrier function (Boncheva, 2014; Damien and Boncheva, 2010). The impact of O₃ on the conformational ordering and

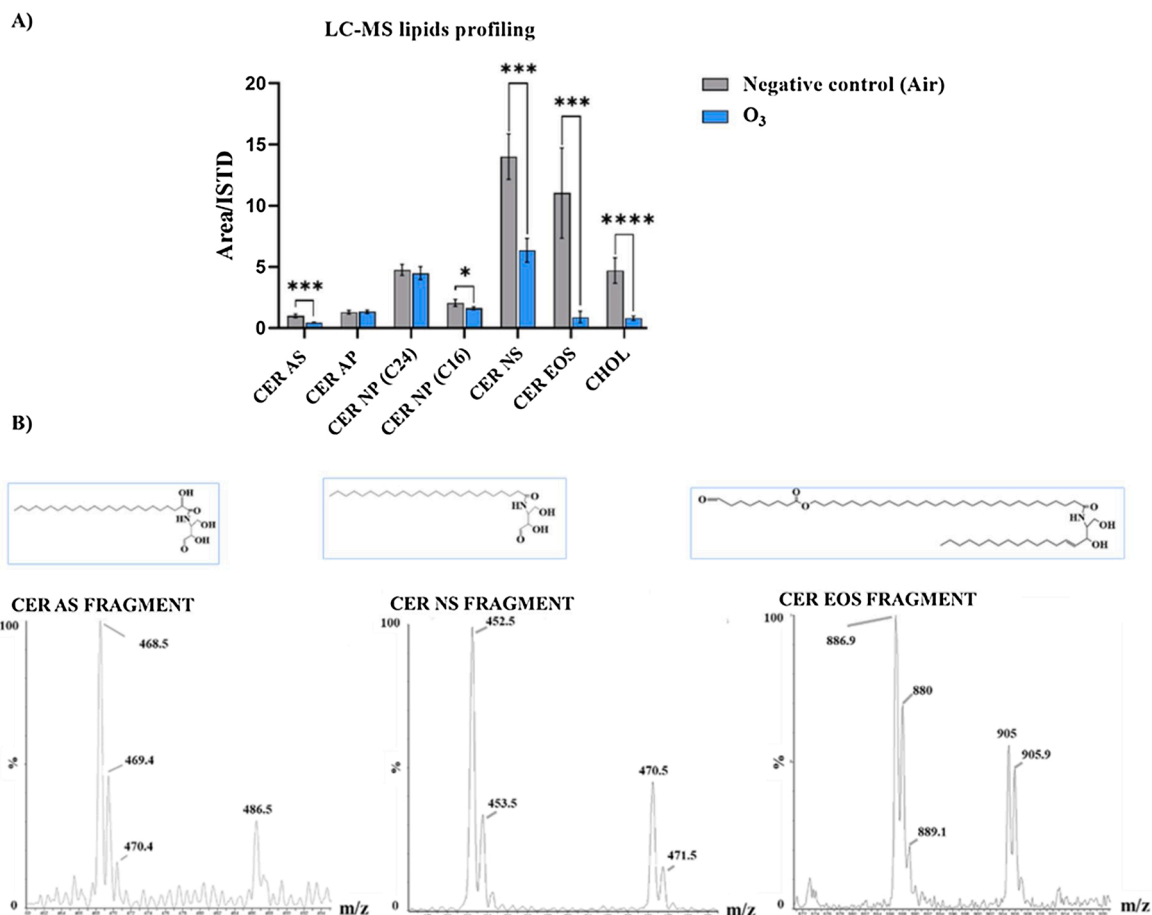


Fig. 2. LC-MS results. A) Ozonolysis of the different CER subclasses and CHOL exposed to air or O₃. Data are presented as a ratio between the AUC of the lipid peak and the AUC of the ISTD peak. *t*-Test. (*) represents P-value (* <0.05 , *** <0.001 and **** <0.0001), $n \geq 3$ per condition. B) Fragments of CER AS, CER NS and CER EOS formed upon O₃ exposure. Y-axis represents the relative intensity of the peaks compared to the highest peak (i.e. 100 %). X-axis represents the m/z .

lipid lateral packing of SCS membranes was investigated by FTIR. The lateral packing adopted by lipid chains can be determined by analysing their δCH_2 and ρCH_2 frequencies in the FTIR spectra. The presence of two peaks in the δCH_2 mode at frequencies of approximately 1463 and 1473 cm^{-1} indicates an ORTH packing (this is due to the interaction of adjacent chains). On the contrary, a singlet observed at around 1467 cm^{-1} indicates that lipids form a HEX packing (Mojumdar et al., 2015). In addition, the doublet ρCH_2 rocking mode indicates the presence of an

ORTH packing in the mixtures, while the presence of a single peak at $\sim 720 \text{ cm}^{-1}$ indicates a HEX phase.

The δCH_2 and ρCH_2 modes spectra were recorded at 10 °C and 32 °C and are illustrated in Fig. 3. At 10 °C the spectra of the samples exposed to air and those exposed to O₃ have two δCH_2 peaks, indicating a predominant ORTH packing. Similar results are observed for ρCH_2 rocking modes in the spectra. At 10 °C both spectra, air and O₃, have two ρCH_2 peaks. These results suggest that O₃ does not affect the lateral lipid

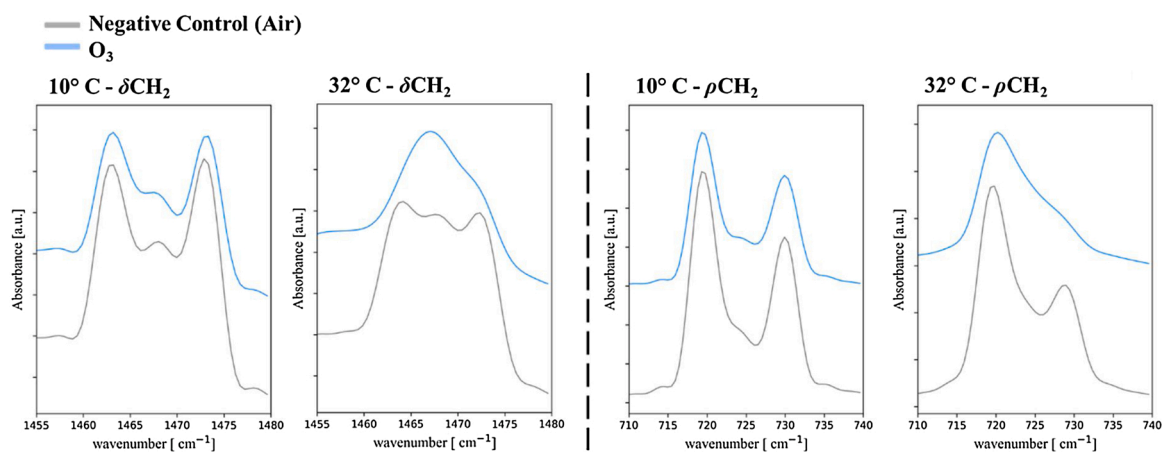


Fig. 3. FTIR spectra at 10 °C and 32 °C of δCH_2 (left) and ρCH_2 (right) modes of the lipid models. Lipid mixtures exposed to O₃ display a less ORTH lateral packing compared to the negative control.

packing at low temperatures.

At 32 °C, the δCH_2 mode of the air exposed samples shows two peaks, although less pronounced than at 10 °C, with a central peak at 1467 cm^{-1} . This indicates that both a HEX and ORTH packing coexist under physiological temperature conditions. The O_3 treated samples exhibits a single broad δCH_2 mode in its spectra, with a small shoulder on the right-hand side. This indicates that the lipids in the O_3 exposed samples are primarily in a HEX phase at 32 °C. A similar observation is made for the ρCH_2 mode. At 32 °C the ρCH_2 mode of the air exposed samples are still characterized by the presence of two peaks, while for the O_3 samples a singlet is present with a shoulder on the right-hand side. Thus, a high fraction of lipids in the O_3 exposed samples adopts a HEX phase at 32 °C, while the air exposed samples show a coexistence of HEX and ORTH lateral packing.

A fitting analysis of the δCH_2 mode, based on Lorentzian functions, was performed to calculate the ratio between the areas of ORTH and HEX peaks (Table 1). A higher ratio demonstrates a higher fraction of lipids in an ORTH lateral packing. This ratio decreases with increasing temperature when the ORTH-HEX transition is occurring. The results at 10 °C show that samples exposed to air and O_3 have similar peak area ratios, thus a similar fraction of lipids forms the ORTH phase. The ratios calculated at 32 °C indicate that the air exposed samples mainly adopt an ORTH phase, while in the O_3 samples an increased population of lipids adopt a HEX phase.

To examine the thermotropic behaviour of SCS membranes in more details, the $\nu_s\text{CH}_2$ mode was also analysed. The $\nu_s\text{CH}_2$ frequency of the hydrocarbon chains provides information about the conformational ordering of the lipid tails (Mojumdar et al., 2014a; Moore et al., 1997). A low wavenumber (below 2850 cm^{-1}) of the $\nu_s\text{CH}_2$ peak indicates the presence of a highly ordered lipid organization (ORTH or HEX), while a higher wavenumber (> 2853 cm^{-1}) indicates a conformational disorder (LIQ). The thermotropic response of the $\nu_s\text{CH}_2$ frequencies of the O_3 and air exposed samples is shown in Fig. 4. At 10 °C, the frequencies of the two curves are below 2850 cm^{-1} . Upon heating of the sample, the $\nu_s\text{CH}_2$ vibration peak shifts toward a higher wavenumber. Two phase transition steps can be identified. The first small step of about 1 cm^{-1} , between 20 °C and 40 °C, suggests an ORTH-HEX phase change. The midpoint temperatures of the ORTH-HEX phase transition ($T_{\text{ORTH-HEX}}$) were calculated. The ORTH-HEX phase transition of the O_3 exposed samples occurs at lower temperatures and over a larger temperature range than the air exposed samples (O_3 $T_{\text{ORTH-HEX}}$ 24.9 ± 4.4 °C vs. air $T_{\text{ORTH-HEX}}$ 33.6 ± 0.6 °C). When increasing the temperature further, the $\nu_s\text{CH}_2$ vibration peak shifts gradually to a higher wavenumber. At higher temperatures, between 50 °C and 70 °C, a second shift of 3 cm^{-1} can be observed, indicating a HEX-LIQ phase transition. The midpoint temperatures of the HEX-LIQ phase transition ($T_{\text{HEX-LIQ}}$) were determined. The HEX-LIQ transition is similar for both exposure conditions (O_3 $T_{\text{HEX-LIQ}}$ 60.5 ± 2.3 °C vs. air $T_{\text{HEX-LIQ}}$ 60.5 ± 2.3 °C) and therefore not sensitive to O_3 exposure.

From these results we conclude that O_3 did not significantly impact the lateral organization of the lipids at low temperatures. However, the O_3 exposed SCS samples shift the ORTH to HEX phase transition temperature to lower values. This might be due to a change in structure of cholesterol, but might also be explained by a change in the headgroup

Table 1

ORTH/HEX peak area ratio calculated from peak fitting analysis. ^(*) represents adjusted P-value, * < 0.05.

SAMPLE	VIBRATION MODE	
	Scissoring δCH_2 ((1463 + 1473)/1467 cm^{-1})	
	10 °C	32 °C
SCS prepared from SC lipids exposed to air	1.3 ± 0.1	1.9 ± 0.4
SCS prepared from SC lipids exposed to O_3	1.1 ± 0.4	0.5 ± 0.4 ^(*)

architecture (Janssens et al., 2009). Hence, the FTIR spectra at the headgroup region (~1650–1750 cm^{-1}) were also analysed (Corbe et al., 2007; Larkin, 2011). Fig. 5 shows the spectra of amide I (~1650 cm^{-1}), and the stretching aldehydic group (~1720–1730 cm^{-1} , the C=O stretching vibration) at 10 °C. In the spectrum of the O_3 exposed samples a more pronounced peak appeared at ~1720 cm^{-1} , indicating the formation of new aldehydic groups upon O_3 exposure.

This result is in agreement with the fragments detected with LC-MS, which are also explained by the presence of a new carbonyl group. Although O_3 does not impact the lateral lipid packing at 10 °C, it modifies the lipid headgroup architecture, which possibly influences the ORTH-HEX transition temperature in our SCS models.

3.3. O_3 does not induce phase separation between CERs and FFAs

To determine whether O_3 influences the spatial arrangement of the SC lipid subclasses into different domains in the SCS model, protiated FFAs were substituted with their deuterated counterparts. The CH_2 and CD_2 vibrations occur at different frequencies, thus changes in their vibrations can be measured simultaneously.

The thermotropic responses of the $\nu_s\text{CH}_2$ and $\nu_s\text{CD}_2$ in both the O_3 and air exposed samples are shown in Fig. 6.

The ORTH-HEX transition is clearly visible in the νCH_2 response, but hardly not in the νCD_2 , caused by the heavier atoms (Gooris and Bouwstra, 2007). In the air exposed samples, both the CERs and DFFAs melted in the same temperature range ($T_{\text{HEX-LIQ}}$ 64.1 ± 0.9 °C for $\nu_s\text{CH}_2$ and $T_{\text{HEX-LIQ}}$ 64.5 ± 0.9 °C for $\nu_s\text{CD}_2$), suggesting no phase separation between those two lipid components. In the O_3 exposed samples, the HEX to LIQ phase transition shows a different behaviour. Whereas the $\nu_s\text{CH}_2$ vibrations led to a single transition in the same temperature range as in the air exposed samples, the $\nu_s\text{CD}_2$ vibrations induced a more complex thermotropic response: the melting of the deuterated FFA chains started at approximately the same temperature as the melting of the protiated chains (i.e. around 60 °C), but then the melting was delayed compared to the protiated chains. At around 82 °C the slope of the curve gradually increased. This indicates that at elevated temperatures the melting process of the protiated and deuterated chains is different. To further understand the spatial arrangement of the lipid classes in our SCS model, it was important to examine whether the deuterated and protiated chains participated in the same lattice at low temperatures. This was evaluated using the corresponding δCD_2 and δCH_2 modes as function of temperature (Fig. 7). The presence of a singlet with maximum at 1088 cm^{-1} is indicative for the participation of FFAs and CERs in one lattice (Groen et al., 2008). Both the air and O_3 exposed samples showed the δCD_2 and δCH_2 modes characterized by a single peak at each temperature. The absence of a clear splitting of the δCD_2 and δCH_2 vibrations indicates a proper mixing of DFFAs and CERs in a single orthorhombic lattice (Gooris and Bouwstra, 2007). Our results suggest that CERs and DFFAs are homogeneously mixed in the SCS models whatever the exposure conditions.

The complex melting process of the DFFAs at high temperatures could result from chemical modifications of SC lipid components (i.e. CHOL and CER EOS) that enhance a proper miscibility (Mojumdar et al., 2015; Uche et al., 2019b). In both the air and O_3 exposed samples, the δCD_2 and δCH_2 spectra show a slight peak broadening that decreases around the ORTH-HEX transition temperature. The broadening of the contour is more evident in the air exposed samples rather than the O_3 exposed ones. Previous studies highlighted the importance of CHOL to enhance the mixing properties of the lipid mixtures (Chen et al., 2001). In our study, it is likely that CHOL can provide a good mixing of CERs and DFFAs despite the changes in its chemical structure upon O_3 exposure.

Our results indicate that O_3 exposure has only a minor effect on the lateral packing and conformational disordering, and that O_3 did not cause a significant phase separation between CERs and FFAs. The next step of our study aimed at evaluating whether O_3 exposure affects the

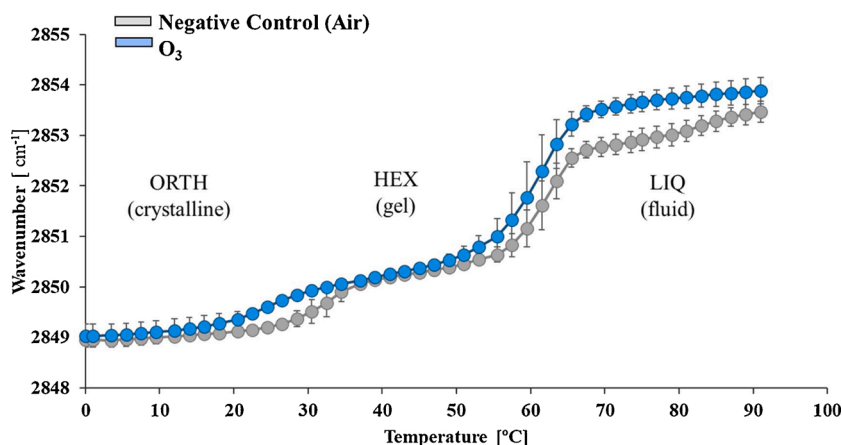


Fig. 4. Thermotropic response of the $\nu_3\text{CH}_2$ modes of the lipid models. O_3 exposed samples show a different ORTH - HEX - LIQ phase transition profile compared to air exposed samples (negative control). The $\nu_3\text{CH}_2$ modes of both models show frequencies below 2850 cm^{-1} at 10°C . However, the ORTH-HEX phase transition of O_3 exposed samples takes place at lower temperatures ($\sim 20\text{--}30^\circ\text{C}$) than the air exposed samples ($\sim 30\text{--}40^\circ\text{C}$). Data presented as mean \pm SD, $n = 3$.

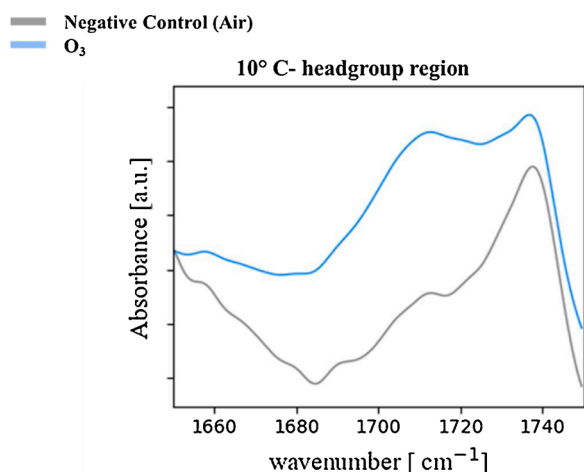


Fig. 5. FTIR spectra of the $1650\text{--}1750\text{ cm}^{-1}$ region at 10°C . Representative of both amide I ($\sim 1650\text{ cm}^{-1}$) and the stretching aldehydic group ($\sim 1720\text{--}1730\text{ cm}^{-1}$, related to the $\text{C}=\text{O}$ stretching vibration).

lamellar phases in the SCS.

3.4. O_3 affects SCS lamellar organization

The effect of O_3 on the lamellar phases of the SCS samples was examined by SAXD. Fig. 8A shows the diffraction pattern of the air exposed samples. Most of the diffraction peaks are attributed to the LPP

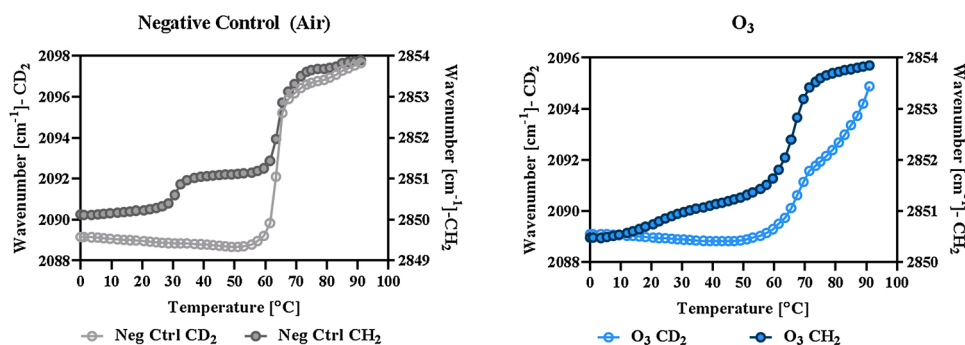


Fig. 6. Thermotropic responses of the νCH_2 and νCD_2 modes of the SCS samples. The CH_2 and CD_2 peak positions are plotted as a function of the temperature for both the air (left) and O_3 (right) exposed samples.

with a calculated repeat distance of 13.4 nm , while two of them can be attributed to crystalline CHOL. Interestingly, the 3rd order diffraction peak has a higher intensity as observed in previous reports (De Jager et al., 2004; Groen et al., 2009). This might indicate the existence of another phase resulting in the same peak position as the 3rd diffraction peak of the LPP. In addition, the diffraction pattern also shows two weak shoulders at $q = 1.53\text{ nm}^{-1}$ and at $q = 2.25\text{ nm}^{-1}$ that suggest the existence of additional phases in the lipid assembly. Whereas the lipid composition used in our study is expected to form only a LPP (Beddoes et al., 2020), the presence of additional phases in our SCS model could result from a partial oxidation of unsaturated lipids exposed to a flow of filtered air for 8 h, even though the LC/MS data analysis did not reveal any fragments upon exposure of the SC lipids to air. Fig. 8B shows the diffraction pattern of the O_3 exposed samples. The diffraction pattern is characterized by the presence of four diffraction orders attributing to a phase with a repeat distance of 8.4 nm . Since the repeat distance is much shorter than that of the traditional LPP and since the intensity distribution of the diffraction peaks is strongly modified, it is likely that the phase formed in the O_3 exposed samples is different to that of the LPP. This hypothesis is in agreement with the oxidation of both CHOL and CER EOS, since those two species are required for the formation of the LPP (De Jager et al., 2004; Mojumdar et al., 2015). Furthermore, all the peaks are very broad indicating disordering of the lamellae. Moreover, the peaks attributed to CHOL could not be detected, probably due to the degradation of CHOL as indicated by the LC-MS data. The weak shoulders at $q = 1.53\text{ nm}^{-1}$ and at $q = 2.25\text{ nm}^{-1}$ detected in the diffraction pattern of the air exposed samples could be associated, respectively, to the second- and third-order peak of the first-order peak at $q = 0.75\text{ nm}^{-1}$ in a lamellar phase. However, the first-order peak at q

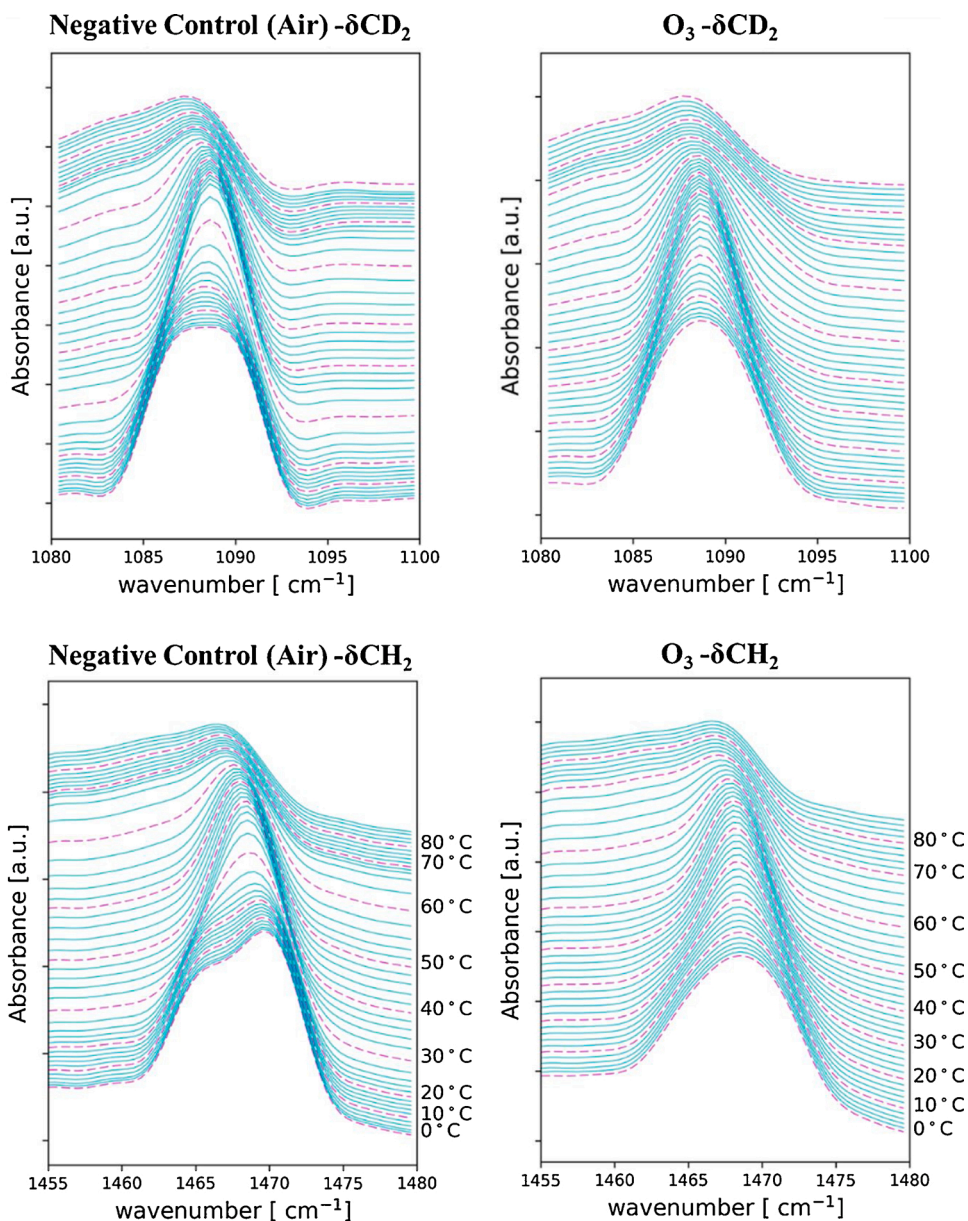


Fig. 7. δCD_2 (top) and δCH_2 (bottom) modes of the SCS samples. The spectra are plotted as a function of temperature for both the air (left) and O_3 (right) exposed samples.

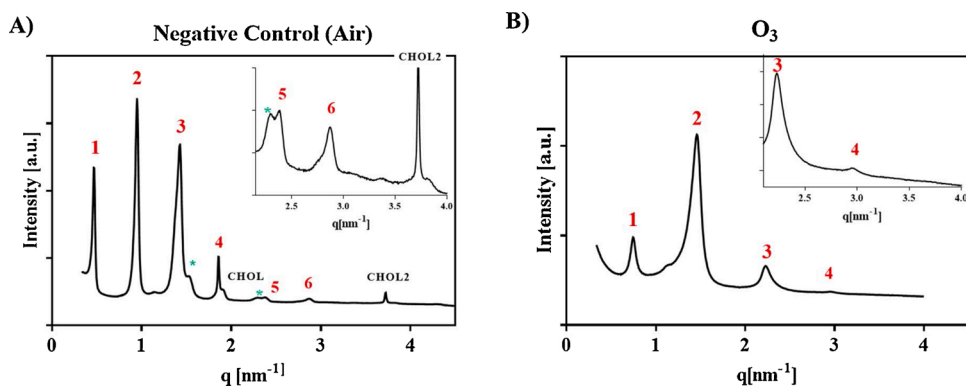


Fig. 8. SAXD profiles of the SCS samples. A) Diffraction profile of the air exposed samples. The numbers indicate the 1st, 2nd, 3rd, 4th, 5th, and 6th order diffraction peaks of the LPP with a repeat distance of 13.4 nm. The two peaks referred to CHOL are indicated in black. Two additional peaks are likely to be present and overlapping the 3rd and 5th peaks of the LPP. Those are indicated by an asterisk (*). B) Diffraction profile of the O_3 exposed samples. The diffraction orders (1, 2, 3 and 4) indicate a repeat distance of 8.4 nm (unknown phase). No peaks attributed to CHOL are present.

= 0.75 nm⁻¹ is present only after O₃ exposure. The absence of the first-order peak in the air exposed samples could result from a slightly different structure in the unit cell.

Our results show that oxidation of unsaturated CERs and CHOL significantly impacts the lamellar lipid organization. These observations are in agreement with studies highlighting that CER EOS and CHOL are crucial for the formation of the LPP (Mojumdar et al., 2015; De Sousa Neto et al., 2011; Schröter et al., 2009; Uche et al., 2021). As the lipid organization was changed upon O₃ exposure, it is of interest to study the effects of O₃ on the barrier properties of the SCS model.

3.5. O₃ affects SCS barrier function

To investigate the effect of O₃ on the SCS barrier function, permeation studies were performed using E-PABA as a model drug. Fig. 9A shows the mean flux profiles of E-PABA through the air and O₃ exposed SCS samples used in this study, while Fig. 9B presents the steady-state flux values. The steady-state flux of E-PABA was significantly lower in SCS composed of lipids exposed to O₃ compared to SCS made of lipids exposed to air only (*p* < 0.0001).

The oxidation of lipid molecules in a membrane system and its consequences on the lateral organization and barrier properties of the lipid assembly have been already reported. A study using molecular dynamic simulations revealed that CHOL oxidation induces both an increase in the molecular area in SC-mimicking lipid bilayers and a decrease in the bilayer thickness which would ultimately result in a reduced barrier efficacy (Yadav et al., 2019). A higher molecular area and a reduction in the thickness are expected to provide a less dense lateral packing. This was not observed with our SC lipid assembly. The membrane model used in the molecular dynamic simulation study was composed of CER NS (C24), FFAs (C24), and CHOL, where the latter was the only component being susceptible to oxidation. Besides, the membrane was intercalated between bulk water. This situation is different from our SCS model where, in addition to CHOL, other lipid components (i.e. CER AS, CER NS and CER EOS) are also prone to oxidation and were found to drastically affect the lipid phase behavior.

Another study also reported the effect of a reduced content of CHOL in mixtures with CERs, CHOL and FFAs on the lipid organization and permeability (Sochorová et al., 2019). They concluded that CHOL depletion had negligible effects on the lateral lipid packing and did not compromise the barrier function to water but increased the permeability of two reference compounds. Interestingly, their membrane model constructed from a mixture of isolated human CERs, FFAs, CHOL, and CHOL sulfate displayed the LPP arrangement even in the absence of CHOL, which may be due to the presence of cholesterol sulfate. In our CHOL-depleted lipid assembly, obtained from SC lipids exposed to O₃, no LPP was observed, which corresponds to previous findings using the same CER composition: the lipids do not form a LPP arrangement in the absence of CHOL (Mojumdar et al., 2015). In the present study, the oxidation products that remain in the assembly seem to reduce the

permeability of E-PABA. This could partially result from CHOL ozonolysis. CHOL enhances the formation of the ORTH packing and the LPP. Therefore, CHOL is important for the skin barrier function. Previous studies showed that both a predominant presence of an ORTH packing and a strong hydrogen bonding in the headgroup region are also of great importance for the barrier properties of skin lipid membrane models (Uche et al., 2019a; Mojumdar et al., 2014a, b). In the present study, since at 32 °C the lipids in the O₃ exposed samples mainly adopt a HEX packing, the reduced permeability of E-PABA cannot be explained by changes in the lateral organization of the lipids in the SCS membrane. However, the changes in the headgroup region enhance the hydrogen bonding between neighbouring lipid molecules, hindering the diffusion of medium lipophilic esters such as E-PABA. Conversely, the decreased diffusion of the model permeant might be explained by the formation of hydrogen bonding, or even by chemical reactions, between E-PABA and the oxidation products of the SC lipids exposed to O₃ (Sprung, 1940).

The linoleate moiety of CER EOS is known to form liquid domains (Bouwstra et al., 2001; Uche et al., 2021). In low concentrations it may entrap diffusing compounds and thus reduce permeability, but at higher concentrations as in our lipid mixture it may form larger liquid domains and increase the permeability (De Jager et al., 2006a; Opálka et al., 2020). Therefore, the degradation of CER EOS, could also contribute to the lower permeability of E-PABA in the O₃ exposed SCS samples.

3.6. How do the O₃ effects observed in the SCS model translate in vivo?

In this work we demonstrated that O₃ oxidizes lipid molecules of the SC extracellular matrix that include olefinic C—C double bonds. These chemical changes significantly impacted the lipid headgroup architecture, the SCS lamellar organization, and to a lesser extent the lateral packing of the lipids. However, they did not weaken the barrier properties of the SCS membrane. These results indicate that exposing our skin to tropospheric O₃ concentrations would not significantly impact the skin barrier function. On the contrary, the O₃ exposed samples were significantly less permeable than the air exposed samples. Nevertheless, an important aspect that was not investigated in this study is the effect of O₃ on the lipids bound to the cornified envelope, which also contains some unsaturated components in the headgroup region (Farwanah et al., 2007; Wertz et al., 1989). The cornified envelope itself might also be affected. Furthermore, O₃ can oxidize many proteins and amino acids (Sharma and Graham, 2010) and several studies have shown that protein carbonyls may be introduced into proteins via reaction with aldehydes (Cotovio et al., 2001; Valacchi et al., 2002). Protein adducts could be formed from the reaction of 4-hydroxy-2-nonenal (i.e. a lipid peroxidation product) with amino acids such as cysteine, lysine and histidine, altering ultimately the protein functions (Pecorelli et al., 2019; Kirichenko et al., 1996). Another important aspect to consider is that there are several unsaturated lipids in sebum (e.g., squalene) present at the skin surface, which may act as scavengers to O₃. The reaction products formed upon sebum oxidation were reported to be skin

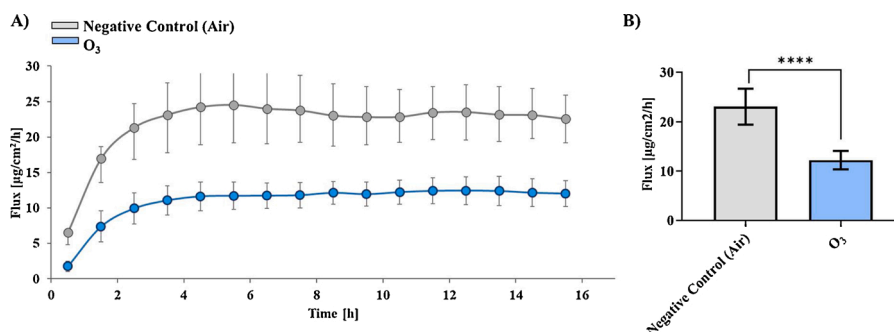


Fig. 9. Barrier properties of the SCS samples. A) Flux of E-PABA across the SCS samples over a 16 h period. B) Average steady-state flux across the SCS. Data presented as mean ± SD, *n* ≥ 4. E-PABA diffusion was significantly lower in SCS composed of O₃ exposed lipids (* represents adjusted P-value, ****<0.0001).

irritants, which could cause damage to the viable epidermis and dermis (Wisthaler and Weschler, 2010).

It has already been reported that O₃ and other pollutants can exacerbate several skin diseases such as atopic eczema and psoriasis (Xu et al., 2011; Ghofranian and Maibach, 2017; Prieux et al., 2020; Hendricks et al., 2020; Dijkhoff et al., 2020). Other studies have shown that next to changes in the SC proteins, these skin diseases are also characterized by an altered SC lipid composition and organization (Van Smeden and Bouwstra, 2016; Van Smeden et al., 2014; Sahle et al., 2015; Ishikawa et al., 2010). In this study, we showed that O₃ exposure modifies both the composition and the biophysical properties of the SC extracellular lipid matrix. It would be of interest to identify possible correlations between those changes induced by O₃ exposure and the development or aggravation of skin diseases. However, the *in vivo* situation is much more complex, as various changes in lipid composition occur simultaneously and a more diverse lipid matrix is present.

4. Conclusions

This work aimed at investigating the effect of a single high dose of O₃ (3.6 ppm for 8 h) on the composition of SC lipids and on their phase behaviour in a multi-layered SCS membrane model. Using the combination of various techniques, we demonstrated that:

- Amongst the various SC lipid molecules used in our SCS model, only the unsaturated CERs (i.e., CER EOS, CER NS and CER AS) and CHOL undergo ozonolysis.
- O₃ induces a change in the lipid headgroup architecture and has only a moderate effect of the lateral lipid packing in the SCS model.
- O₃ induces the formation of a less-ordered lamellar phase with a shorter repeat distance (~8.4 nm) than the so-characteristic LPP (~13 nm).
- The changes in SC lipid composition, in lipid headgroup architecture and in SCS lamellar organization do not seem to weaken the barrier properties of the multi-layered model, as the diffusion of E-PABA, a lipophilic ester compound, is reduced.

This study set the basis for understanding the effects of O₃ on SC lipids and the consequence on lipid organization and barrier function. More insights about the effects of single and chronic O₃ exposure on SC lipids might help to identify possible correlations between skin diseases and ambient air pollution.

Transparency document

The [Transparency document](#) associated with this article can be found in the online version.

Declaration of Competing Interest

The authors report no declarations of interest.

Acknowledgments

This research article has been written as part of the CITYCARE project which has received funding from the European Union's Horizon 2020 research and innovation program under the Marie Skłodowska-Curie grant agreement [grant number 765602]. Benedetta Petracca acknowledges the support of the Adolphe Merkle Foundation. We thank the company Evonik for the donation of the ceramides and the ALBA synchrotron light facility for their assistance during the X-ray diffraction experiments.

References

- Bailey, P.S., 1958. The reactions of ozone with organic compounds. *Chem. Rev.* 58 (5), 925–1010. <https://doi.org/10.1021/cr50023a005>.
- Beddoes, C.M., Gooris, G.S., Bouwstra, J.A., 2018. Preferential arrangement of lipids in the long-periodicity phase of a stratum corneum matrix model. *J. Lipid Res.* 59 (12), 2329–2338. <https://doi.org/10.1194/jlr.M087106>.
- Beddoes, C.M., Gooris, G.S., Foglia, F., Ahmadi, D., Barlow, D.J., Lawrence, M.J., Demé, B., Bouwstra, J.A., 2020. Arrangement of ceramides in the skin: sphingosine chains localize at a single position in stratum corneum lipid matrix models. *Langmuir* 36 (34), 10270–10278. <https://doi.org/10.1021/acs.langmuir.0c01992>.
- Bocci, V., 2010. Physical-chemical properties of ozone – natural production of ozone: the toxicology of ozone. In: Springer Science & Business Media (Ed.), *OZONE A New Medical Drug*. Springer, Netherlands: Dordrecht, pp. 1–4. https://doi.org/10.1007/978-90-481-9234-2_1.
- Boiten, W., Absalah, S., Vreeken, R., Bouwstra, J., van Smeden, J., 2016. Quantitative analysis of ceramides using a novel lipidomics approach with three dimensional response modelling. *Biochim. Biophys. Acta - Mol. Cell Biol. Lipids* 1861 (11), 1652–1661. <https://doi.org/10.1016/j.bbalip.2016.07.004>.
- Boncheva, M., 2014. The physical chemistry of the stratum corneum lipids. *Int. J. Cosmet. Sci.* 36 (6), 505–515. <https://doi.org/10.1111/ics.12162>.
- Bouwstra, J.A., Gooris, G.S., van der Spek, J.A., Bras, W., 1991. Structural investigations of human stratum corneum by small-angle X-ray scattering. *J. Invest. Dermatol.* 97 (6), 1005–1012. <https://doi.org/10.1111/1523-1747.ep12492217>.
- Bouwstra, J.A., Gooris, G.S., Cheng, K., Weerheim, A., Bras, W., Ponec, M., 1996. Phase behavior of isolated skin lipids. *J. Lipid Res.* 37 (5), 999–1011.
- Bouwstra, J.A., Gooris, G.S., Dubbelaar, F.E.R., Ponec, M., 2001. Phase behavior of lipid mixtures based on human ceramides: coexistence of crystalline and liquid phases. *J. Lipid Res.* 42 (11), 1759–1770. [https://doi.org/10.1016/S0022-2275\(20\)31502-9](https://doi.org/10.1016/S0022-2275(20)31502-9).
- Caussin, J., Gooris, G.S., Janssens, M., Bouwstra, J.A., 2008. Lipid organization in human and porcine stratum corneum differs widely, while lipid mixtures with porcine ceramides model human stratum corneum lipid organization very closely. *Biochim. Biophys. Acta Biomembr.* 1778 (6), 1472–1482. <https://doi.org/10.1016/j.bbamem.2008.03.003>.
- Chen, H.C., Mendelsohn, R., Rerek, M.E., Moore, D.J., 2001. Effect of cholesterol on miscibility and phase behavior in binary mixtures with synthetic ceramide 2 and octadecanoic acid. Infrared studies. *Biochim. Biophys. Acta Biomembr.* 1512 (2), 345–356. [https://doi.org/10.1016/S0005-2736\(01\)00339-X](https://doi.org/10.1016/S0005-2736(01)00339-X).
- Corbe, E., Laugel, C., Yagoubi, N., Baillat, A., 2007. Role of ceramide structure and its microenvironment on the conformational order of model stratum corneum lipids mixtures: an approach by FTIR spectroscopy. *Chem. Phys. Lipids* 146 (2), 67–75. <https://doi.org/10.1016/j.chemphyslip.2006.12.010>.
- Cotovio, J., Onno, L., Justine, P., Lamure, S., Catroux, P., 2001. Generation of oxidative stress in human cutaneous models following *in vitro* ozone exposure. *Toxicol. In Vitro* 15 (4–5), 357–362. [https://doi.org/10.1016/S0887-2333\(01\)00036-4](https://doi.org/10.1016/S0887-2333(01)00036-4).
- Criegee, R., 1975. Mechanism of ozonolysis. *Angew. Chemie Int. Ed. English* 14 (11), 745–752. <https://doi.org/10.1002/anie.197507451>.
- Cross, C.E., Valacchi, G., Schock, B., Wilson, M., Weber, S., Eiserich, J., Van der Vliet, A., 2002. Environmental oxidant pollutant effects on biologic systems: a focus on micronutrient antioxidant-oxidant interactions. *Am. J. Respir. Crit. Care Med.* 166 (12 II) <https://doi.org/10.1164/rccm.2206015>.
- Damien, F., Boncheva, M., 2010. The extent of orthorhombic lipid phases in the stratum corneum determines the barrier efficiency of human skin *in vivo*. *J. Invest. Dermatol.* 130 (2), 611–614. <https://doi.org/10.1038/jid.2009.272>.
- De Jager, M.W., Gooris, G.S., Dolbnya, I.P., Ponec, M., Bouwstra, J.A., 2004. Modelling the stratum corneum lipid organisation with synthetic lipid mixtures: the importance of synthetic ceramide composition. *Biochim. Biophys. Acta Biomembr.* 1664 (2), 132–140. <https://doi.org/10.1016/j.bbamem.2004.05.001>.
- De Jager, M.W., Gooris, G.S., Ponec, M., Bouwstra, J.A., 2005. Lipid mixtures prepared with well-defined synthetic ceramides closely mimic the unique stratum corneum lipid phase behavior. *J. Lipid Res.* 46 (12), 2649–2656. <https://doi.org/10.1194/jlr.M500221-JLR200>.
- De Jager, M., Groenink, W., Bielsa I Guivernau, R., Andersson, E., Angelova, N., Ponec, M., Bouwstra, J., 2006a. A novel *in vitro* percutaneous penetration model: evaluation of barrier properties with P-aminobenzoic acid and two of its derivatives. *Pharm. Res.* 23 (5), 951–960. <https://doi.org/10.1007/s11095-006-9909-1>.
- De Jager, M., Groenink, W., van der Spek, J., Janmaat, C., Gooris, G., Ponec, M., Bouwstra, J., 2006b. Preparation and characterization of a stratum corneum substitute for *in vitro* percutaneous penetration studies. *Biochim. Biophys. Acta Biomembr.* 1758 (5), 636–644. <https://doi.org/10.1016/j.bbamem.2006.04.001>.
- De Sousa Neto, D., Gooris, G., Bouwstra, J., 2011. Effect of the ω -acylceramides on the lipid organization of stratum corneum model membranes evaluated by X-ray diffraction and FTIR studies (Part I). *Chem. Phys. Lipids* 164 (3), 184–195. <https://doi.org/10.1016/j.chemphyslip.2010.12.007>.
- Dijkhoff, I.M., Drasler, B., Karakocak, B.B., Petri-Fink, A., Valacchi, G., Eeman, M., Rothen-Rutishauser, B., 2020. Impact of airborne particulate matter on skin: a systematic review from epidemiology to *in vitro* studies. *Part. Fibre Toxicol.* 17 (1), 1–28. <https://doi.org/10.1186/s12989-020-00366-y>.
- Drakaki, E., Dessinioti, C., Antoniou, C.V., 2014. Air pollution and the skin. *Front. Environ. Sci.* 2 (May), 1–6. <https://doi.org/10.3389/fenvs.2014.00011>.
- Elias, P.M., 2005. Stratum corneum defensive functions: an integrated view. *J. Invest. Dermatol.* 125 (2), 183–200. <https://doi.org/10.1111/j.0022-202X.2005.23668.x>.
- Farwanah, H., Pierstorff, B., Schmelzer, C.E.H., Raith, K., Neubert, R.H.H., Kolter, T., Sandhoff, K., 2007. Separation and mass spectrometric characterization of covalently bound skin ceramides using LC/APCI-MS and Nano-ESI-MS/MS.

- J. Chromatogr. B Anal. Technol. Biomed. Life Sci. 852 (1–2), 562–570. <https://doi.org/10.1016/j.jchromb.2007.02.030>.
- Feng, Z., Hu, E., Wang, X., Jiang, L., Liu, X., 2015. Ground-level O₃ pollution and its impacts on food crops in China: a review. *Environ. Pollut.* 199, 42–48. <https://doi.org/10.1016/j.envpol.2015.01.016>.
- Fuks, K.B., Woodby, B., Valacchi, G., 2019. Skin damage by tropospheric ozone. *Der Hautarzt* 70 (3), 163–168. <https://doi.org/10.1007/s00105-019-4361-4>.
- Ghofrani, A., Maibach, H.I., 2017. Effects of air pollution on skin. *Cosmetic Science and Technology*. Elsevier, pp. 757–766. <https://doi.org/10.1016/B978-0-12-802005-0.00047-1>.
- Gooris, G.S., Bouwstra, J.A., 2007. Infrared spectroscopic study of stratum corneum model membranes prepared from human ceramides, cholesterol, and fatty acids. *Biophys. J.* 92 (8), 2785–2795. <https://doi.org/10.1529/biophysj.106.094292>.
- Gooris, G.S., Kamran, M., Kros, A., Moore, D.J., Bouwstra, J.A., 2018. Interactions of dipalmitoylphosphatidylcholine with ceramide-based mixtures. *Biochim. Biophys. Acta Biomembr.* 1860 (6), 1272–1281. <https://doi.org/10.1016/j.bbmem.2018.02.024>.
- Groen, D., Gooris, G.S., Ponc, M., Bouwstra, J.A., 2008. Two new methods for preparing a unique stratum corneum substitute. *Biochim. Biophys. Acta Biomembr.* 1778 (10), 2421–2429. <https://doi.org/10.1016/j.bbmem.2008.06.015>.
- Groen, D., Gooris, G.S., Bouwstra, J.A., 2009. New insights into the stratum corneum lipid organization by X-ray diffraction analysis. *Biophys. J.* 97 (8), 2242–2249. <https://doi.org/10.1016/j.bpj.2009.07.040>.
- Groen, D., Gooris, G.S., Bouwstra, J.A., 2010. Model membranes prepared with ceramide EOS, cholesterol and free fatty acids form a unique lamellar phase. *Langmuir* 26 (6), 4168–4175. <https://doi.org/10.1021/la9047038>.
- Hendricks, A.J., Eichenfield, L.F., Shi, V.Y., 2020. The impact of airborne pollution on atopic dermatitis: a literature review. *Br. J. Dermatol.* 183 (1), 16–23. <https://doi.org/10.1111/bjd.18781>.
- Ishikawa, J., Narita, H., Kondo, N., Hotta, M., Takagi, Y., Masukawa, Y., Kitahara, T., Takema, Y., Koyano, S., Yamazaki, S., Hatamochi, A., 2010. Changes in the ceramide profile of atopic dermatitis patients. *J. Invest. Dermatol.* 130 (10), 2511–2514. <https://doi.org/10.1038/jid.2010.161>.
- Janssens, M., Gooris, G.S., Bouwstra, J.A., 2009. Infrared spectroscopy studies of mixtures prepared with synthetic ceramides varying in head group architecture: coexistence of liquid and crystalline phases. *Biochim. Biophys. Acta Biomembr.* 1788 (3), 732–742. <https://doi.org/10.1016/j.bbmem.2009.01.003>.
- Kirichenko, A., Li, L., Morandi, M.T., Holian, A., 1996. 4-hydroxy-2-nonenal-protein adducts and apoptosis in murine lung cells after acute ozone exposure. *Toxicol. Appl. Pharmacol.* 141 (2), 416–424. <https://doi.org/10.1006/TAAP.1996.0307>.
- Krieg, P., Rosenberger, S., de Juanes, S., Latzko, S., Hou, J., Dick, A., Klotz, U., van der Hoeven, F., Hauser, I., Esposito, I., Rauh, M., Schneider, H., 2013. Alox3 knockout mice reveal a function of epidermal lipoxygenase-3 as hepxilin synthase and its pivotal role in barrier formation. *J. Invest. Dermatol.* 133 (1), 172–180. <https://doi.org/10.1038/jid.2012.250>.
- Krutmann, J., Bouloc, A., Sore, G., Bernard, B.A., Passeron, T., 2017. The skin aging exposome. *J. Dermatol. Sci.* 85 (3), 152–161. <https://doi.org/10.1016/j.jdermsci.2016.09.015>.
- Larkin, P., 2011. Illustrated IR and Raman spectra demonstrating important functional groups. *Infrared and Raman Spectroscopy*. Elsevier, pp. 135–176. <https://doi.org/10.1016/B978-0-12-386984-5.10008-4>.
- Masukawa, Y., Narita, H., Sato, H., Naoue, A., Kondo, N., Sugai, Y., Oba, T., Homma, R., Ishikawa, J., Takagi, Y., Kitahara, T., 2009. Comprehensive quantification of ceramide species in human stratum corneum. *J. Lipid Res.* 50 (8), 1708–1719. <https://doi.org/10.1194/jlr.D800055-JLR200>.
- Meguro, S., Arai, Y., Masukawa, Y., Uie, K., Tokimitsu, I., 2000. Relationship between covalently bound ceramides and transepidermal water loss (TEWL). *Arch. Dermatol. Res.* 292 (9), 463–468. <https://doi.org/10.1007/s004030000160>.
- Mojumdar, E.H., Helder, R.W.J., Gooris, G.S., Bouwstra, J.A., 2014a. Monounsaturated fatty acids reduce the barrier of stratum corneum lipid membranes by enhancing the formation of a hexagonal lateral packing. *Langmuir* 30 (22), 6534–6543. <https://doi.org/10.1021/la500972w>.
- Mojumdar, E.H., Kariman, Z., van Kerckhove, L., Gooris, G.S., Bouwstra, J.A., 2014b. The role of ceramide chain length distribution on the barrier properties of the skin lipid membranes. *Biochim. Biophys. Acta - Biomembr.* 1838 (10), 2473–2483. <https://doi.org/10.1016/j.bbmem.2014.05.023>.
- Mojumdar, E.H., Gooris, G.S., Bouwstra, J.A., 2015. Phase behavior of skin lipid mixtures: the effect of cholesterol on lipid organization. *Soft Matter* 11 (21), 4326–4336. <https://doi.org/10.1039/C4SM02786H>.
- Moore, D.J., Rerek, M.E., Mendelsohn, R., 1997. FTIR spectroscopy studies of the conformational order and phase behavior of ceramides. *J. Phys. Chem. B* 101 (44), 8933–8940. <https://doi.org/10.1021/jp9718109>.
- Norlén, L., Nicander, L., Lundsjö, A., Cronholm, T., Forslind, B., 1998. A new HPLC-based method for the quantitative analysis of inner stratum corneum lipids with special reference to the free fatty acid fraction. *Arch. Dermatol. Res.* 290 (9), 508–516. <https://doi.org/10.1007/s004030050344>.
- Oguri, M., Gooris, G.S., Bito, K., Bouwstra, J.A., 2014. The effect of the chain length distribution of free fatty acids on the mixing properties of stratum corneum model membranes. *Biochim. Biophys. Acta Biomembr.* 1838 (7), 1851–1861. <https://doi.org/10.1016/j.bbmem.2014.02.009>.
- Ohta, N., Ban, S., Tanaka, H., Nakata, S., Hatta, I., 2003. Swelling of intercellular lipid lamellar structure with short repeat distance in hairless mouse stratum corneum as studied by X-ray diffraction. *Chem. Phys. Lipids* 123 (1), 1–8. [https://doi.org/10.1016/S0009-3084\(02\)00126-3](https://doi.org/10.1016/S0009-3084(02)00126-3).
- Opálka, L., Kováčik, A., Maixner, J., Vávrová, K., 2016. Omega-O-acylceraimides in skin lipid membranes: effects of concentration, sphingoid base, and model complexity on microstructure and permeability. *Langmuir* 32 (48), 12894–12904. <https://doi.org/10.1021/acs.langmuir.6b03082>.
- Opálka, L., Kováčik, A., Pullmannová, P., Maixner, J., Vávrová, K., 2020. Effects of omega-O-acylceraimide structures and concentrations in healthy and diseased skin barrier lipid membrane models. *J. Lipid Res.* 61 (2), 219–228. <https://doi.org/10.1194/jlr.RA119000420>.
- Pecorelli, A., Woodby, B., Prieux, R., Valacchi, G., 2019. Involvement of 4-hydroxy-2-nonenal in pollution-induced skin damage. *BioFactors* 45 (4), 536–547. <https://doi.org/10.1002/biof.1513>.
- Petracca, B., Rothen-Rutishauser, B., Valacchi, G., Eeman, M., 2021. Bench approaches to study the detrimental cutaneous impact of tropospheric ozone. *J. Expo. Sci. Environ. Epidemiol.* 31 (1), 137–148. <https://doi.org/10.1038/s41370-020-00275-4>.
- Pilgram, G.S.K., Marjolein Engelsma-van Pelt, A., Koerten, H.K., Bouwstra, J.A., 1999. Electron diffraction provides new information on human stratum corneum lipid organization studied in relation to depth and temperature. *J. Invest. Dermatol.* 113 (3), 403–409. <https://doi.org/10.1046/j.1523-1747.1999.00706.x>.
- Pouillot, A., Dayan, N., Polla, A.S., Polla, L.L., Polla, B.S., 2008. The stratum corneum: a double paradox. *J. Cosmet. Dermatol.* 7 (2), 143–148. <https://doi.org/10.1111/j.1473-2165.2008.00379.x>.
- Prieux, R., Eeman, M., Rothen-Rutishauser, B., Valacchi, G., 2020. Mimicking cigarette smoke exposure to assess cutaneous toxicity. *Toxicol. In Vitro* 62 (July 2019), 104664. <https://doi.org/10.1016/j.tiv.2019.104664>.
- Pryor, W.A., 1992. How far does ozone penetrate into the pulmonary air/tissue boundary before it reacts? *Free Radic. Biol. Med.* 12 (1), 83–88. [https://doi.org/10.1016/0891-5849\(92\)90060-T](https://doi.org/10.1016/0891-5849(92)90060-T).
- Pryor, W.A., Church, D.F., 1991. Aldehydes, hydrogen peroxide, and organic radicals as mediators of ozone toxicity. *Free Radic. Biol. Med.* 11 (1), 41–46. [https://doi.org/10.1016/0891-5849\(91\)90186-7](https://doi.org/10.1016/0891-5849(91)90186-7).
- Pryor, W.A., Squadrito, G.L., Friedman, M., 1995a. A new mechanism for the toxicity of ozone. *Toxicol. Lett.* 82–83, 287–293. [https://doi.org/10.1016/0378-4274\(95\)03563-X](https://doi.org/10.1016/0378-4274(95)03563-X), 1995.
- Pryor, W.A., Squadrito, G.L., Friedman, M., 1995b. A new mechanism for the toxicity of ozone. *Toxicol. Lett.* 82–83, 287–293, 1995.
- Pryor, W.A., Squadrito, G.L., Friedman, M., 1995c. The cascade mechanism to explain ozone toxicity: the role of lipid ozonation products. *Free Radic. Biol. Med.* 19 (6), 935–941. [https://doi.org/10.1016/0891-5849\(95\)02033-7](https://doi.org/10.1016/0891-5849(95)02033-7).
- Rabionet, M., Gorgas, K., Sandhoff, R., 2014. Ceramide synthesis in the epidermis. *Biochim. Biophys. Acta - Mol. Cell Biol. Lipids* 1841 (3), 422–434. <https://doi.org/10.1016/j.bbalip.2013.08.011>.
- Rasmussen, C., Gratz, K., Liebel, F., Southall, M., Garay, M., Bhattacharyya, S., Simon, N., Zanden, M., Vander, Winkle, K., Van, Pirnstill, J., Pirnstill, S., Comer, A., Allen-Hoffmann, B.L., 2010. The StrataTest® human skin model, a consistent in vitro alternative for toxicological testing. *Toxicol. In Vitro* 24 (7), 2021–2029. <https://doi.org/10.1016/j.tiv.2010.07.027>.
- Sahle, F.F., Gebre-Mariam, T., Dobner, B., Wohlrab, J., Neubert, R.H.H., 2015. Skin diseases associated with the depletion of stratum corneum lipids and stratum corneum lipid substitution therapy. *Skin Pharmacol. Physiol.* 28 (1), 42–55. <https://doi.org/10.1159/000360009>.
- Schröter, A., Kessner, D., Kiselev, M.A., Hauß, T., Dante, S., Neubert, R.H.H., 2009. Basic nanostructure of stratum corneum lipid matrices based on ceramides [EOS] and [AP]: a neutron diffraction study. *Biophys. J.* 97 (4), 1104–1114. <https://doi.org/10.1016/j.bpj.2009.05.041>.
- Sharma, V.K., Graham, N.J.D., 2010. Oxidation of amino acids, peptides and proteins by ozone: a review. *Ozone Sci. Eng.* 32 (2), 81–90. <https://doi.org/10.1080/01919510903510507>.
- Shelley, W.B., 1992. Physiology, biochemistry, and molecular biology of the skin. *JAMA J. Am. Med. Assoc.* 268 (4), 545. <https://doi.org/10.1001/jama.1992.03490040129042>.
- Sochorová, M., Audrlická, P., Cervená, M., Kováčik, A., Kopečná, M., Opálka, L., Pullmannová, P., Vávrová, K., 2019. Permeability and microstructure of cholesterol-depleted skin lipid membranes and human stratum corneum. *J. Colloid Interface Sci.* 535, 227–238. <https://doi.org/10.1016/j.jcis.2018.09.104>.
- Sprung, M.A., 1940. A summary of the reactions of aldehydes with amines. *Chem. Rev.* 26 (3), 297–338. <https://doi.org/10.1021/cr60085a001>.
- Swartzendruber, D.C., Wertz, P.W., Madison, K.C., Downing, D.T., 1987. Evidence that the corneocyte has a chemically bound lipid envelope. *J. Invest. Dermatol.* 88 (6), 709–713. <https://doi.org/10.1111/1523-1747.ep12470383>.
- T'Kindt, R., Jorge, L., Dumont, E., Couturon, P., David, F., Sandra, P., Sandra, K., 2012. Profiling and characterizing skin ceramides using reversed-phase liquid chromatography-quadrupole time-of-flight mass spectrometry. *Anal. Chem.* 84 (1), 403–411. <https://doi.org/10.1021/ac202646v>.
- Thiele, J., Traber, M.G., Polefka, T.G., Cross, C.E., Packer, L., 1997. Ozone-exposure depletes vitamin E and induces lipid peroxidation in murine stratum corneum. *J. Invest. Dermatol.* 108 (5), 753–757. <https://doi.org/10.1111/1523-1747.ep12292144>.
- Trommer, H., 2001. The examination of skin lipid model systems stressed by ultraviolet irradiation in the presence of transition metal ions. *Eur. J. Pharm. Biopharm.* 51 (3), 207–214. [https://doi.org/10.1016/S0939-6411\(01\)00140-0](https://doi.org/10.1016/S0939-6411(01)00140-0).
- Trommer, H., Plätzer, M., Wolf, R., Neubert, R.H.H., 2003. Mass spectrometric examinations of stratum corneum lipid models exposed to ultraviolet irradiation. *Skin Pharmacol. Physiol.* 16 (5), 291–304. <https://doi.org/10.1159/000072069>.
- Uche, L.E., Gooris, G.S., Beddoes, C.M., Bouwstra, J.A., 2019a. New insight into phase behavior and permeability of skin lipid models based on sphingosine and phytosphingosine ceramides. *Biochim. Biophys. Acta Biomembr.* 1861 (7), 1317–1328. <https://doi.org/10.1016/j.bbmem.2019.04.005>.

- Uche, L.E., Gooris, G.S., Bouwstra, J.A., Beddoes, C.M., 2019b. Barrier capability of skin lipid models: effect of ceramides and free fatty acid composition. *Langmuir* 35 (47), 15376–15388. <https://doi.org/10.1021/acs.langmuir.9b03029>.
- Uche, L.E., Gooris, G.S., Bouwstra, J.A., Beddoes, C.M., 2021. High concentration of the ester-linked ω -hydroxy ceramide increases the permeability in skin lipid model membranes. *Biochim. Biophys. Acta - Biomembr.* 1863 (1), 183487. <https://doi.org/10.1016/j.bbmem.2020.183487>.
- Valacchi, G., 2010. Effect of ozone on cutaneous tissues. In: *Textbook of Aging Skin*, Vol. 70. Springer, Berlin Heidelberg: Berlin, Heidelberg, pp. 411–420. https://doi.org/10.1007/978-3-540-89656-2_41.
- Valacchi, G., van der Vliet, A., Schock, B., Okamoto, T., Obermuller-Jevic, U., Cross, C., Packer, L., 2002. Ozone exposure activates oxidative stress responses in murine skin. *Toxicology* 179 (1–2), 163–170. [https://doi.org/10.1016/S0300-483X\(02\)00240-8](https://doi.org/10.1016/S0300-483X(02)00240-8).
- Valacchi, G., Pagnin, E., Corbacho, A.M., Olano, E., Davis, P.A., Packer, L., Cross, C.E., 2004. In vivo ozone exposure induces antioxidant/stress-related responses in murine lung and skin. *Free Radic. Biol. Med.* 36 (5), 673–681. <https://doi.org/10.1016/j.freeradbiomed.2003.12.005>.
- Valacchi, G., Sticozzi, C., Pecorelli, A., Cervellati, F., Cervellati, C., Maioli, E., 2012. Cutaneous responses to environmental stressors. *Ann. N. Y. Acad. Sci.* 1271 (1), 75–81. <https://doi.org/10.1111/j.1749-6632.2012.06724.x>.
- Van Smeden, J., Bouwstra, J.A., 2016. Stratum corneum lipids: their role for the skin barrier function in healthy subjects and atopic dermatitis patients. In: *Skin Barrier Function*, vol. 49, pp. 8–26. <https://doi.org/10.1159/000441540>.
- Van Smeden, J., Hoppel, L., Van Der Heijden, R., Hankemeier, T., Vreeken, R.J., Bouwstra, J.A., 2011. LC/MS analysis of stratum corneum lipids: ceramide profiling and discovery. *J. Lipid Res.* 52 (6), 1211–1221. <https://doi.org/10.1194/jlr.M014456>.
- Van Smeden, J., Janssens, M., Gooris, G.S., Bouwstra, J.A., 2014. The important role of stratum corneum lipids for the cutaneous barrier function. *Biochim. Biophys. Acta - Mol. Cell Biol. Lipids* 1841 (3), 295–313. <https://doi.org/10.1016/j.bbalip.2013.11.006>.
- Wertz, P.W., Miethke, M.C., Long, S.A., Strauss, J.S., Downing, D.T., 1985. The composition of the ceramides from human stratum corneum and from comedones. *J. Invest. Dermatol.* 84 (5), 410–412. <https://doi.org/10.1111/1523-1747.ep12265510>.
- Wertz, P.W., Madison, K.C., Downing, D.T., 1989. Covalently bound lipids of human stratum corneum. *J. Invest. Dermatol.* 92 (1), 109–111. <https://doi.org/10.1111/1523-1747.ep13071317>.
- Wisthaler, A., Weschler, C.J., 2010. Reactions of ozone with human skin lipids: sources of carbonyls, dicarbonyls, and hydroxycarbonyls in indoor air. *Proc. Natl. Acad. Sci.* 107 (15), 6568–6575. <https://doi.org/10.1073/pnas.0904498106>.
- Xu, F., Yan, S., Wu, M., Li, F., Xu, X., Song, W., Zhao, J., Xu, J., Kan, H., 2011. Ambient ozone pollution as a risk factor for skin disorders. *Br. J. Dermatol.* 165 (1), 224–225. <https://doi.org/10.1111/j.1365-2133.2011.10349.x>.
- Yadav, D.K., Kumar, S., Choi, E.H., Chaudhary, S., Kim, M.H., 2019. Molecular dynamic simulations of oxidized skin lipid bilayer and permeability of reactive oxygen species. *Sci. Rep.* 9 (1), 1–10. <https://doi.org/10.1038/s41598-019-40913-y>.